Journal of Hazardous Materials 168 (2009) 253–261

Contents lists available at ScienceDirect

Journal of Hazardous Materials

journal homepage: www.elsevier.com/locate/jhazmat

Visible light absorption ability and photocatalytic oxidation activity of various interstitial N-doped TiO_2 prepared from different nitrogen dopants

Jirapat Ananpattarachai [a], Puangrat Kajitvichyanukul [b,c,*], Supapan Seraphin [d]

[a] Department of Environmental Engineering, King Mongkut's University of Technology Thonburi, Bangkok 10140, Thailand
[b] Biological Engineering Program, King Mongkut's University of Technology Thonburi, Bangkok 10140, Thailand
[c] National Center of Excellence for Environmental and Hazardous Waste Management, KMUTT Satellite Center, King Mongkut's University of Technology Thonburi, Bangkok 10140, Thailand
[d] Department of Materials Science and Engineering, University of Arizona, Tucson, AZ 85721, USA

ARTICLE INFO

Article history:
Received 9 October 2008
Received in revised form 5 February 2009
Accepted 6 February 2009
Available online 20 February 2009

Keywords:
N-doped TiO_2
TiO_2
Photocatalyst
Visible light
2-Chlorophenol
Degradation
Oxidation

ABSTRACT

Nitrogen-doped TiO_2 was developed to enable photocatalytic reactions using the visible range of the solar spectrum. This work reports on the synthesis, characterisation and kinetic study of interstitial N-doped TiO_2 prepared by the sol–gel method using three different types of nitrogen dopants: diethanolamine, triethylamine and urea. X-ray diffraction, scanning electron microscopy, transmission electron microscopy, X-ray photoelectron spectroscopy and UV–visible spectroscopy were used to analyse the titania. Different interstitial N-doped TiO_2 properties, such as absorption ability in the UV–visible light region, redshift in adsorption edge, good crystallisation and composition ratio of titania structures (anatase and rutile) could be obtained from different nitrogen dopants. Amongst investigated nitrogen precursors, diethanolamine provided the highest visible light absorption ability of interstitial N-doped TiO_2 with the smallest energy bandgap and the smallest anatase crystal size, resulting in the highest efficiency in 2-chlorophenol degradation. The photocatalytic activity of all N-doped TiO_2 can be arranged in the following order: TiO_2/diethanolamine > TiO_2/triethylamine > TiO_2/urea > un-doped TiO_2. The initial rate of 2-chlorophenol degradation using the interstitial N-doped TiO_2 with diethanolamine was 0.59 mg/L-min and the kinetic constant was 2.34×10^{-2} min^{-1} with a half-life of 98 min. In all cases, hydroquinone was detected as a major intermediate in the degradation of 2-chlorophenol.

1. Introduction

Titanium dioxide (TiO_2), an example of metal-oxide type semiconductors, has been studied and widely used as a photocatalytic material for self-cleaning coatings, environmental purifiers, antifogging mirrors and many other applications [1]. TiO_2 has a bandgap of 3.0 eV for the rutile phase and 3.2 eV for the anatase phase. These values require ultraviolet (UV) radiation to activate. Recently, many attempts have been made to make TiO_2 highly reactive under visible light excitation to allow utilisation of the solar spectrum [2]. A new method using anion-doped systems to obtain the visible light-activated TiO_2 has been reported [3]. Some anionic species such as nitrogen, carbon and sulphur were identified to potentially form new impurity levels closest to the valence band whilst maintaining the largest bandgap for maximum efficiency. Many previous works indicated that doping TiO_2 with nitrogen is one of the most effective approaches in improving properties and photocatalytic activity of TiO_2 in visible light regions [3,4]. Nitrogen can incorporate into the TiO_2 structure as substitutionals and as interstitials. X-ray photoelectron spectroscopy (XPS) is used to determine binding energy of the sample surface states to identify whether doped nitrogen was incorporated as substitutionals or interstitials. If XPS spectra show N 1s peaks at 396–398 eV, the Ti–N–Ti linkages are substitutional N-doped TiO_2. If, however, the N 1s peaks are at 400–406 eV, the characters of Ti–O–N and/or Ti–N–O indicate interstitial N-doped TiO_2. Recently, Peng et al. demonstrated that the visible light activity of interstitial N-doped TiO_2 is higher than that of substitutional N-doped TiO_2 [5]. However, to date, little research has gone into obtaining in-depth information on the properties of the interstitial N-doped TiO_2, as well as its photocatalytic activity.

Different nitrogen dopants have been employed to obtain several complexes of the N-doped TiO_2. These dopants result in TiO_2 with different properties, and consequently alter the photocatalytic activity of the obtained materials. Currently, less work has focused

* Corresponding author at: Biological Engineering Program, King Mongkut's University of Technology Thonburi, 126 Pracha-Utid Rd., Bangkok 10140, Thailand. Tel.: +66 2 4707583; fax: +66 2 4707583.
E-mail addresses: kpuangrat@yahoo.com, puangrat.kaj@kmutt.ac.th (P. Kajitvichyanukul).

0304-3894/$ – see front matter © 2009 Elsevier B.V. All rights reserved.
doi:10.1016/j.jhazmat.2009.02.036

on the effects of nitrogen dopants added in sol–gel solutions than on the properties of N-doped TiO_2 [6]. Applications of N-doped TiO_2 for the removal of various types of organic pollutants from the environment such as acetaldehyde [7], methylcyclohexene [8], benzoic acid [9] and methyl orange [10] have recently reported. However, to enhance the practicability in applying this TiO_2 species to the environmental application, more research in this area must be performed.

The principal aims of this work were to synthesise visible-light-sensitive TiO_2 powders with interstitial molecular structures using different types of nitrogen dopants and to investigate effects of nitrogen dopants on the degradation of an organic pollutant. The three investigated dopants were diethanolamine (DEA), triethylamine (TEN) and urea. To test the photocatalytic activity of the obtained interstitial N-doped TiO_2, 2-chlorophenol (2-CP) was selected as an organic probe due to its high toxicity and its wide use in many industrial activities. In this work, authors investigated the alterations of interstitial N-doped TiO_2 properties, such as strong absorption in the UV–visible (UV–vis) light region, redshift in adsorption edge, degree of crystallisation and mixture of two phase structures (anatase and rutile) of the titania obtained from different dopants. Degradation and mineralisation of 2-chlorphenol using each type of interstitial N-doped TiO_2 were determined. Relations between properties of the N-doped TiO_2 and kinetic parameters in the photocatalytic degradation of 2-chlorophenol were also examined in this work.

2. Materials and methods

2.1. Materials

All reagents used were of analytical grade and employed as received. Titanium tetraisopropoxide (TTiP), 2-chlorophenol (2-CP), ammonium chloride (NH_4Cl), ammonium hydroxide solution (NH_4OH), 4-aminoantipyrine ($C_{11}H_{13}N_3O$) and potassium ferricyanide ($K_3Fe(CN)_6$) were purchased from Aldrich Chemicals. Ethanol (EtOH), nitric acid (HNO_3), sulphuric acid (H_2SO_4) and sodium hydroxide (NaOH) were obtained from Merck Chemicals. Nitrogen dopants including diethanolamine (DEA), triethylamine (TEN) and urea were from Acros Organics, and 18 MΩ deionised water (H_2O) was used to prepare the solutions.

2.2. TiO_2 catalyst synthesis

A modified sol–gel method was used to synthesise N-doped TiO_2 with a mole ratio of 1:20:1:1:1 for TTiP:EtOH:HNO_3:H_2O:dopant (DEA, TEN or urea). First, TTiP was dissolved in EtOH, and the solution was stirred for 30 min. In a second solution, EtOH was mixed with H_2O that contained HNO_3. This solution was stirred to promote hydrolysis until transparent. After mixing both portions, precipitation readily occurred. The dopant was then added to the solution. For comparison, TiO_2 without a dopant was prepared using the same method (labelled as un-doped TiO_2). The homogeneous transparent solution was then kept under stirring conditions for 30 min at 4 °C before undergoing the drying process. After drying at 100 °C for 90 min, the powder was collected and calcined at 800 °C in an electric tube furnace in a N_2 atmosphere. The samples were held at the peak temperature for 30 min and then cooled to room temperature. A commercial grade Degussa P-25 TiO_2 powder was used as a reference.

2.3. TiO_2 catalyst characterisation

All N-doped TiO_2 samples were analysed by a Philips X-ray diffractometer using Cu Kα radiation and a step size of 0.02° in the range of 20–70°. The step time was 1 s, adequate to obtain a good signal-to-noise ratio in the mean reflections of the two main TiO_2 crystalline phases, (1 0 1) anatase ($2\theta - 25.281°$) and (1 1 0) rutile ($2\theta - 27.495°$). The average crystallite size of anatase was determined according to the Scherrer equation using the full-width at half-maximum (FWHM) of the (1 0 1) or (1 1 0) peak and taking into account the instrument broadening. Scanning electron microscopy (SEM) studies were performed with a field emission Hitachi S-4500 SEM operated at 15 kV to examine the morphology of the nanoparticles. Transmission electron microscope (TEM) studies were performed using a Hitachi H-8100 TEM operated at 200 kV to study the size, shape and crystallinity of the nanoparticles. The optical absorption spectra of the samples were obtained by measuring their diffuse reflectance spectra in a Perkin Elmer UV/vis Lambda 35 spectrophotometer and then converting to absorbance units by using the Kubelka–Munk theory. The absorption spectra of the powder were measured using an integrating sphere (Lambda 35 (P/N C6951014)) to capture the scattered light from a sample in powder sample holder set (P/N B0505835). The measurement was performed in absorbance mode, scanning from 200 to 800 nm using a 2-nm slit. X-ray photoelectron spectroscopy (XPS) spectra were attained with a KRATOS 165 ULTRA photoelectron spectrometer with either an Al Kα or Mg Kα monochromatic source. The BET surface areas were measured by nitrogen adsorption–desorption isotherms at 77 K with a Quantachrome AUTOSORB-1.

2.4. Photochemical reaction

Photocatalysis experiments were performed in a batch reactor. The reactor was cylindrical with a volume of 1.1 L made from quartz glass (ACE Glass Co. 7841-06; Vineland, NJ). The visible light source was a 150 W halogen lamp (Sylvania). A solution containing 1 M sodium nitrite was used as a UV-filter [11,12] to eliminate light <420 nm. The initial concentration of 2-CP was 25 mg/L, and the catalyst was 1 g/L. In this photocatalytic experiment, the 2-CP solution was injected into the reactor and treated in batch operation mode with a steady temperature maintained at 25 ± 2 °C throughout the experiment in an oxygen atmosphere. The liquid was allowed to equilibrate in the dark for 30 min. After reaching equilibrium, the reaction was started by switching on the light at $t = 0$, and the initial concentration of 2-CP was designated as C_0. In the photocatalytic experiment, the pH value was adjusted to 7.0 by adding concentrated sulphuric acid to the photoreaction. The solution was well aerated and fully stirred with a magnetic stirrer to ensure sufficient mixing. At a chosen interval of irradiation time, aliquots of the reaction mixture were withdrawn and filtered with a membrane filter (0.1 μm). To determine 2-CP concentration, the sample solutions were subsequently reacted with 4-aminoantipyrine at pH 7.9 ± 0.1 in the presence of potassium ferricyanide to form a coloured antipyrine dye. This dye was kept in aqueous solution, and the absorbance was measured at 510 nm by a Lambda 35 PerkinElmer UV–vis spectrometer [13]. The concentration of 2-CP at each sampling time was designated as C. The reaction period for all experiments in this work was 50 min unless otherwise specified. For identification of intermediate products from 2-CP irradiated solutions after 50 min, the sample was analysed by a Clarus 600 PerkinElmer gas chromatograph equipped with a mass selective detector (Clarus 600T Mass Spectrometer). The GC column

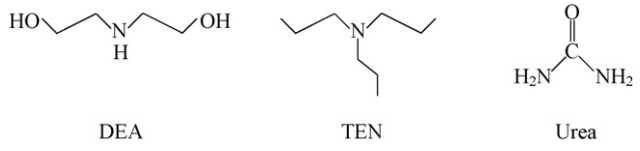

Fig. 1. Molecular structures of diethanolamine (DEA), triethylamine (TEN) and urea.

employed was a PE-1HT (0.25 mm i.d., 30 m) column (PerkinElmer) with 0.1 mm film thickness. The GCMS operating conditions and the extraction procedure have been described elsewhere [14].

3. Results and discussion

3.1. Characteristics of investigated N-doped TiO_2

Molecular structures of three investigated dopants are shown in Fig. 1. Urea has a carbonyl group flanked by two primary amines. DEA is a secondary amine with a dialcohol. TEN has three alkyl branches and is considered a tertiary amine. These differences in the basic character of the dopant caused significantly different characteristics and properties of each N-doped TiO_2 as described below.

3.1.1. X-ray diffraction

X-ray diffraction was used to determine the phase composition of the samples, weight fractions of each phase and crystallite size. Fig. 2 shows the effects of nitrogen dopants on the phase compositions of the N-doped TiO_2 powders calcined at 800 °C. As shown in the X-ray diffraction patterns of TiO_2 nanoparticles, the anatase phase was the predominant structure in N-doped TiO_2 under all synthesis conditions. A major peak corresponding to (1 0 1) reflections of the anatase phase of TiO_2 was apparent at the angle of 25.28°, whilst the minor peaks appeared at 37.80°, 48.05°, 53.89° and 55.06°. The rutile phase can be found from un-doped TiO_2, TiO_2/TEN and TiO_2/urea with the major peak of the (1 1 0) diffraction at the angle of 27.50°, whilst the minor peaks appeared at 36.15°, 41.33°, 54.44°, 56.76°, 62.89° and 69.17°. X-ray diffraction analysis of all samples revealed that only TiO_2 obtained from DEA dopant had typical peaks of TiO_2 anatase without any detectable peaks of rutile. We also found that the anatase structure from this nitrogen dopant was retained up to 1000 °C. Weight fractions of each phase were calculated by the following equation:

$$W_R = \frac{A_R}{0.884A_A + A_R},$$

where A_A represents the integrated intensity of the anatase (1 0 1) peak and A_R the integrated intensity of the rutile (1 1 0) peak [15].

The average particle size was estimated by applying the Scherrer's formula on the anatase (1 0 1) and rutile (1 1 0) diffraction peaks (the highest intensity peak of each phase):

$$L = \frac{K\lambda}{\beta \cos\theta},$$

where L is the crystallite size, K a constant (usually 0.89), λ the wavelength of the X-ray radiation (0.15418 nm for Cu Kα), β the line width at half-maximum height and θ is the corresponding diffraction angle in degrees.

Weight fractions of phase, estimated crystal size and surface area from BET analysis of all N-doped TiO_2 samples are listed in Table 1. Weight fractions of each phase and the crystal size of titania powders changed greatly depending on nitrogen dopant. DEA provided the smallest crystal size of anatase, whilst urea apparently increased the crystal size of this phase. DEA can reduce anatase crystal size of titania from 12.02 nm (un-doped TiO_2) down to 4.86 nm. However, the corresponding surface area of each titania catalyst was not significantly different. Weight fractions of anatase of TiO_2/TEN and TiO_2/urea were also slightly elevated compared to un-doped TiO_2.

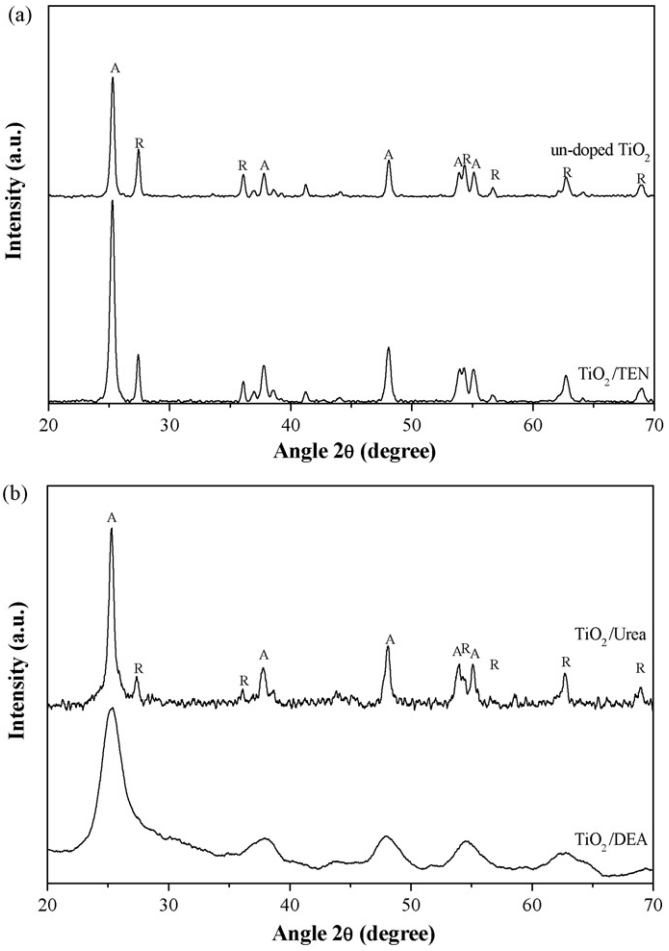

Fig. 2. XRD spectra showing crystal structures of N-doped TiO_2. A is anatase; R is rutile.

3.1.2. Scanning electron microscopy

Morphologies of N-doped TiO_2 revealed by SEM micrographs are shown in Fig. 3. All samples appeared as agglomerations of smaller particles. Cluster sizes of the as-synthesised catalyst were strongly dependent on the type of nitrogen dopant. The TiO_2 powder in all cases presented aggregates consisting of smaller particles (100 nm for TiO_2/TEN) to larger particles (about 500 nm for TiO_2/DEA) with a high tendency for crystallisation. Fine particles with a very homogeneous size distribution can be seen in TiO_2/urea.

TEM images (Fig. 4) of N-doped TiO_2 show significant differences amongst the studied samples. The anatase phase in TiO_2/DEA was in a uniform dimension with an average crystal size of about

Table 1
Crystal size and surface area of all N-doped TiO_2 calcined at 800 °C.

N-doped TiO_2	Weight fractions of phase (%)		Crystal size (nm)			Surface area (m^2/g)
	Anatase	Rutile	Anatase	Rutile	Average	
Un-doped TiO_2	66	34	12.02	20.77	14.99	11.78
TiO_2/DEA	100	–	4.86	–	4.86	9.84
TiO_2/TEN	77	23	8.22	15.29	9.84	10.23
TiO_2/urea	86	14	20.83	17.86	20.42	11.25

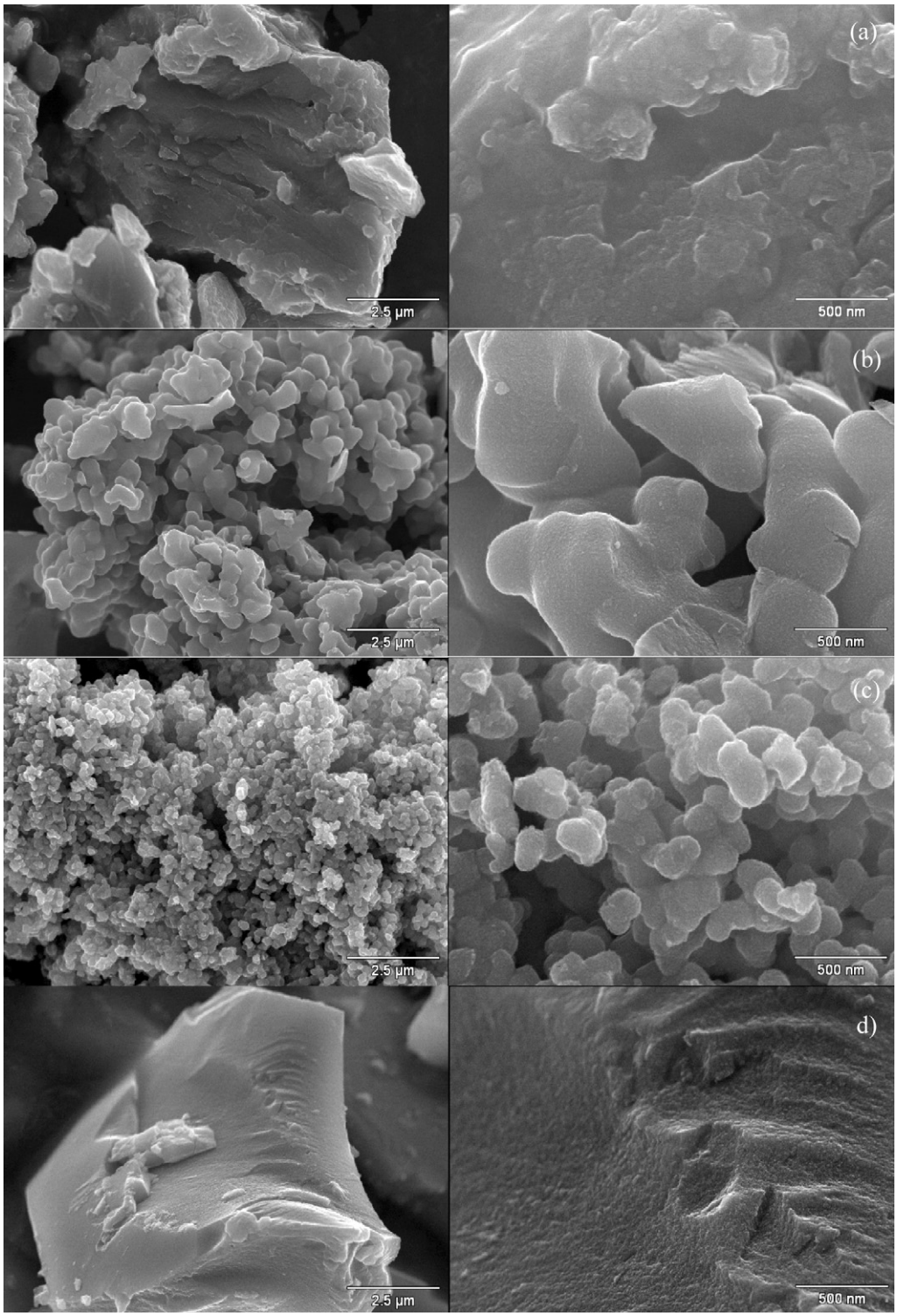

Fig. 3. SEM micrographs of different types of N-doped TiO_2: (a) un-doped TiO_2, (b) TiO_2/DEA, (c) TiO_2/TEN and (d) TiO_2/urea. Images on the right were taken at higher magnification than the one on the left.

4–5 nm, and no rutile phase was detected. The mixed anatase and rutile phase was clearly present in un-doped TiO_2, TiO_2/TEN and TiO_2/urea. The crystallite sizes observed in the TEM micrographs were consistent with those obtained from the estimation of peak broadening of XRD spectra. The smallest crystal size of the anatase phase from TiO_2/DEA was approximately 5 nm, and the larger particles of the rutile phase from all types of N-doped TiO_2 exceeded an average of 10 nm.

3.1.3. UV–vis spectroscopy

Fig. 5 shows the UV–vis spectra of four different types of N-doped TiO_2 powders and the reference TiO_2 (Degussa, P-25). This figure illustrates the response of the N-doped TiO_2 to visible light (400–800 nm wavelength). P-25 has higher absorption in UV region (200–300 nm) than the other TiO_2, but no significant absorption in the visible light region. The un-doped TiO_2 and TiO_2/TEN have high absorption in the UV region but relatively low absorption in visi-

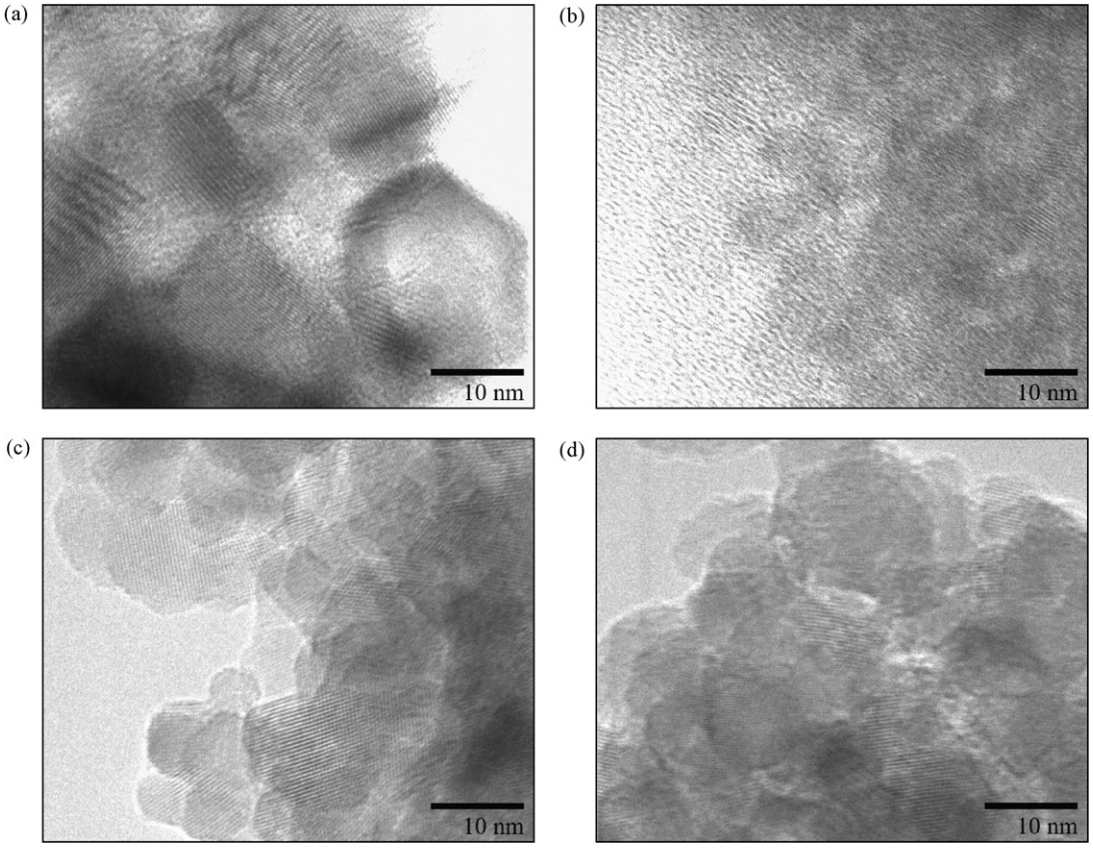

Fig. 4. TEM micrographs of different types of N-doped TiO_2: (a) un-doped TiO_2, (b) TiO_2/DEA, (c) TiO_2/TEN and (d) TiO_2/urea.

ble light region compared to TiO_2/urea and TiO_2/DEA. Amongst all types of investigated TiO_2, TiO_2/DEA provided the highest visible light absorption ability. This result indicates that the investigated nitrogen dopants effectively extended absorption of TiO_2 into the visible light range. As shown in Fig. 5, the absorption in the visible light region of un-doped TiO_2 is relatively low. In addition, TiO_2 synthesised with organic materials under air atmosphere at same temperature also provided no significant absorption in the visible light region. This information suggests that organic materials introduced the nitrogen to N-doped TiO_2 under the nitrogen atmosphere reaction and visible light absorption ability is mainly dependent on the type of nitrogen dopant. The bandgap energy of un-doped and N-doped TiO_2 can be estimated from plots of the square root of Kubelka–Munk functions $F(R)$ versus photon energy [2]. The relation of $(\alpha h\nu)^2$ and $(h\nu)$ was plotted. The bandgap of TiO_2 can be determined from the following equation:

$$\alpha h\nu = A(h\nu - E_g)^r,$$

where A is a constant, $h\nu$ the photon energy, E_g the optical energy gap of the material and r is the characteristic of the type of the optical transition process, which is equal to 2.0 for an indirect allowed optical transition of an amorphous semiconductor. Bandgap energies of the investigated N-doped TiO_2 are summarised in Table 2.

Table 2
Bandgap energy of various types of N-doped TiO_2.

N-doped TiO_2	Bandgap (eV)
P-25	3.20
Un-doped TiO_2	3.16
TiO_2/DEA	2.85, 3.08
TiO_2/TEN	3.05, 3.20
TiO_2/urea	3.10, 3.20

Results show that bandgap energies of all N-doped TiO_2 were lower than those of un-doped TiO_2 and P-25. The bandgap changed from 3.20 eV (P-25) to 2.85 and 3.08 for TiO_2/DEA, 3.05 and 3.20 for TiO_2/TEN and 3.10 and 3.20 for TiO_2/urea. The first bandgap reflects the effect of N-doping on the main band edges of the oxide. The second gap, which is narrower than the original value, suggests that nitrogen doping contributed to the redshift of the bandgap. This narrower bandgap will facilitate excitation of electrons from the valence band to the conduction band in the doped oxide semiconductor under visible light illumination, which can result in higher photocatalytic activities.

3.1.4. X-ray photoelectron spectroscopy (XPS)

The XPS spectra of un-doped TiO_2 and three N-doped TiO_2 samples are shown in Fig. 6. The surfaces of all N-doped TiO_2 samples are composed of titania, oxygen, nitrogen and carbon contaminants. No nitrogen signal was detected in the un-doped TiO_2 sample whilst weak nitrogen signals appeared in all N-doped TiO_2 samples. The insets in Fig. 6 show enlarged N 1s peaks of the corresponding XPS spectra. The intensities of the N 1s peaks of TiO_2/DEA and TiO_2/urea were more pronounced than the weak intensities of TiO_2/TEN. The 401.3 eV binding energy of N 1s was detected in TiO_2/DEA only; 402.5 eV was detected in TiO_2/DEA, TiO_2/TEN and TiO_2/urea; 406.1 eV was detected in TiO_2/DEA and TiO_2/urea; and 409.7 eV was detected in TiO_2/urea only. From previous works [10,16–21], typical binding energies of less than 397.5 eV are assigned to TiN species mostly in substitutional N, whilst N 1s peaks at binding energies above 400 eV are usually attributed to NO or NO_2, characteristic of interstitial N. Thus, all N-doped TiO_2 obtained from this work are classified as interstitial N-doped TiO_2. The proposed structure of this type of titania is described by the binding of a nitrogen atom to an oxygen lattice in the environment of O–Ti–N and/or Ti–N–O,

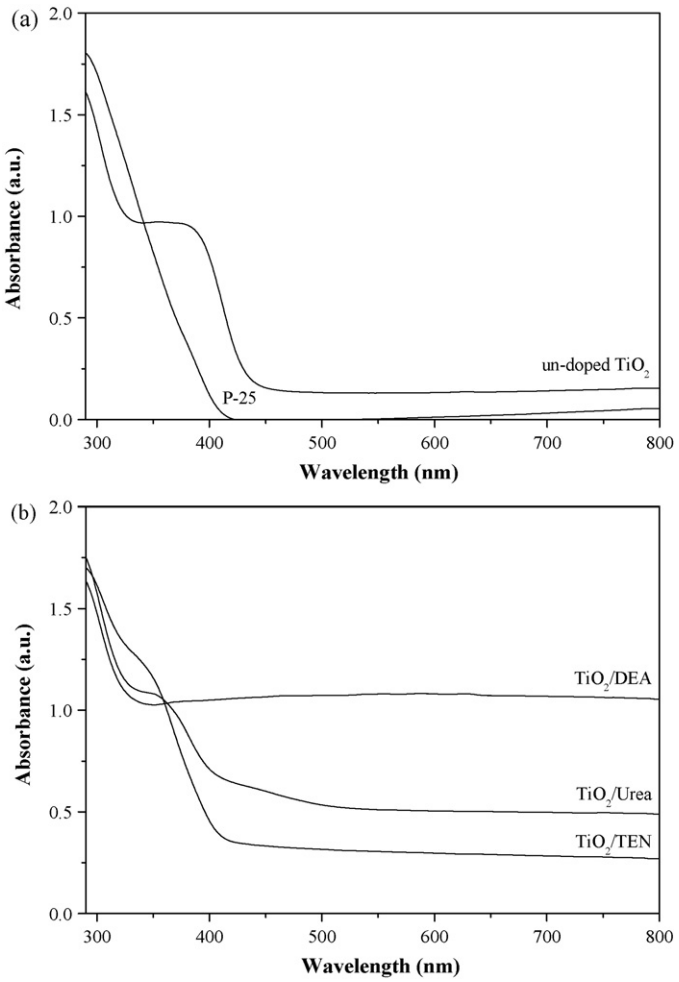

Fig. 5. UV–vis absorption spectra of four types of N-doped TiO_2 and the reference TiO_2 (P-25).

and the nitrogen has a positive oxidation state [19]. Peaks appearing at binding energies of 402.5 eV and 406.1 eV have been assigned to nitric oxide, or nitrogen monoxide (NO), and nitrite (NO_2^-), respectively [20,21]. This NO bond generates localised states with a π characteristic and has the highest localised state for interstitial species [19]. Our work suggests that different nitrogen dopants can provide different types of NO bonding in N-doped TiO_2 synthesised under the same processing conditions. The bonding of NO can be found in all investigated nitrogen dopants. However, DEA and urea generate NO bonding in the form of nitrite (NO_2^-) species. This information indicated that nitrogen from both DEA and urea is effectively doped into the titania.

Percentage of nitrogen content in N-doped TiO_2, as well as the atomic ratios of Ti:N, Ti:O and O:N atomic ratios, are presented in Table 3. Urea with a primary amine structure is anticipated to introduce the highest amount of nitrogen to the catalyst as seen from the highest percentage of nitrogen content and lowest atomic ratio of Ti:N. By the same consideration, TEN as a tertiary amine provided less nitrogen atoms to the titania. This information suggests that the chemical composition (N content) of N-doped TiO_2 largely depends on the molecular structure of the nitrogen dopant and the accessibility of nitrogen atoms to react with the titania precursor. Furthermore, primary and secondary amines are promising chemicals to provide the N-rich catalyst material.

Table 3
Ti:N, Ti:O, O:N atomic ratios, and %N content of N-doped TiO_2 samples obtained from XPS.

N-doped TiO_2	Atomic ratio			%N content
	Ti:N	Ti:O	O:N	
Un-doped TiO_2	–	0.35	–	0.00
TiO_2/DEA	4.47	0.36	12.48	4.11
TiO_2/TEN	23.33	0.32	72.50	0.64
TiO_2/urea	0.34	0.06	5.93	5.01

3.2. Kinetics study of 2-chlorophenol removal using N-doped TiO_2

To investigate the ability of interstitial N-doped TiO_2 to remove a hazardous pollutant from the wastewater, synthesised TiO_2 was used in the photocatalysis process of 2-CP degradation in aqueous solution. In general, the photocatalytic reaction involves different processes including adsorption–desorption, electron–hole pair production and recombination and chemical conversion [22]. Since the recombination of photogenerated electron–hole pairs occurs within a fraction of a nanosecond, charge separation is only kinetically competitive if trapping species are already adsorbed prior to electron–hole pair generation [23–25]. Consequently, in this work, the photocatalytic activity of nanocrystal TiO_2 was divided into two parts, the adsorption and irradiation processes.

3.2.1. Adsorption of 2-chlorophenol

Preliminary adsorption experiments revealed that in the absence of TiO_2, no noticeable change in 2-CP concentration occurred during a 30-min experimental period. Adsorption of 2-CP using all synthesised N-doped TiO_2 was evaluated, and the highest concentrations of adsorbed 2-CP on different types of TiO_2 surfaces were determined. Results of this experiment are shown in Fig. 7. The contact time to reach equilibrium was approximately 5 min for un-doped TiO_2, TiO_2/TEN and TiO_2/urea. Roughly, 20 min was required for TiO_2/DEA to reach equilibrium. Equilibrium concentrations of 2-CP in aqueous solution after treatment with all four types of N-doped TiO_2 were not significantly different. In all cases, Degussa P-25 TiO_2 powder provided the highest adsorption of 2-CP onto the titania surface owing to its highest surface area, 55 m^2/g compared to a range of 9–12 m^2/g for other types of N-doped TiO_2. The adsorbed 2-CP under equilibrium conditions using N-doped TiO_2 ranged from 7 to 9 mg 2-CP/g TiO_2 or approximately 28% removals.

3.2.2. Visible light irradiation of 2-chlorophenol

To explore the photocatalytic activity of N-doped TiO_2 in the visible range, degradation of 2-CP by visible light was investigated. The photocatalytic behaviour of un-doped TiO_2 was also measured as a control. Notably, 2-CP was confirmed to be reasonably photostable in aqueous solution under irradiation by light in the 315–400 nm wavelength range, whilst it underwent fast photolysis when irradiated at 254 nm [26,27]. Results from this study showed that 2-CP degradation through direct photolysis in the visible light range was negligible (<4%). Therefore, the degradation of 2-CP after treating with the N-doped TiO_2 was likely due to the photocatalysis of the N-doped TiO_2.

The photocatalytic reactivity of various types of N-doped TiO_2 was represented by the ratio of residual concentration to initial concentration of 2-CP, C/C_0, as a function of irradiation time. As illustrated in Fig. 8, different N-doped TiO_2 catalysts behaved differently in the degradation of 2-CP under the same experimental conditions for a period of 50 min. Clearly, the degradation of 2-CP increased with irradiation time duration. However, the trend of 2-CP degradation is apparently different for different catalysts. Amongst all types of investigated TiO_2, TiO_2/DEA provided the highest photoefficiency for 2-CP degradation. The highest photocatalytic activity of the N-doped TiO_2 with DEA might have been partially due

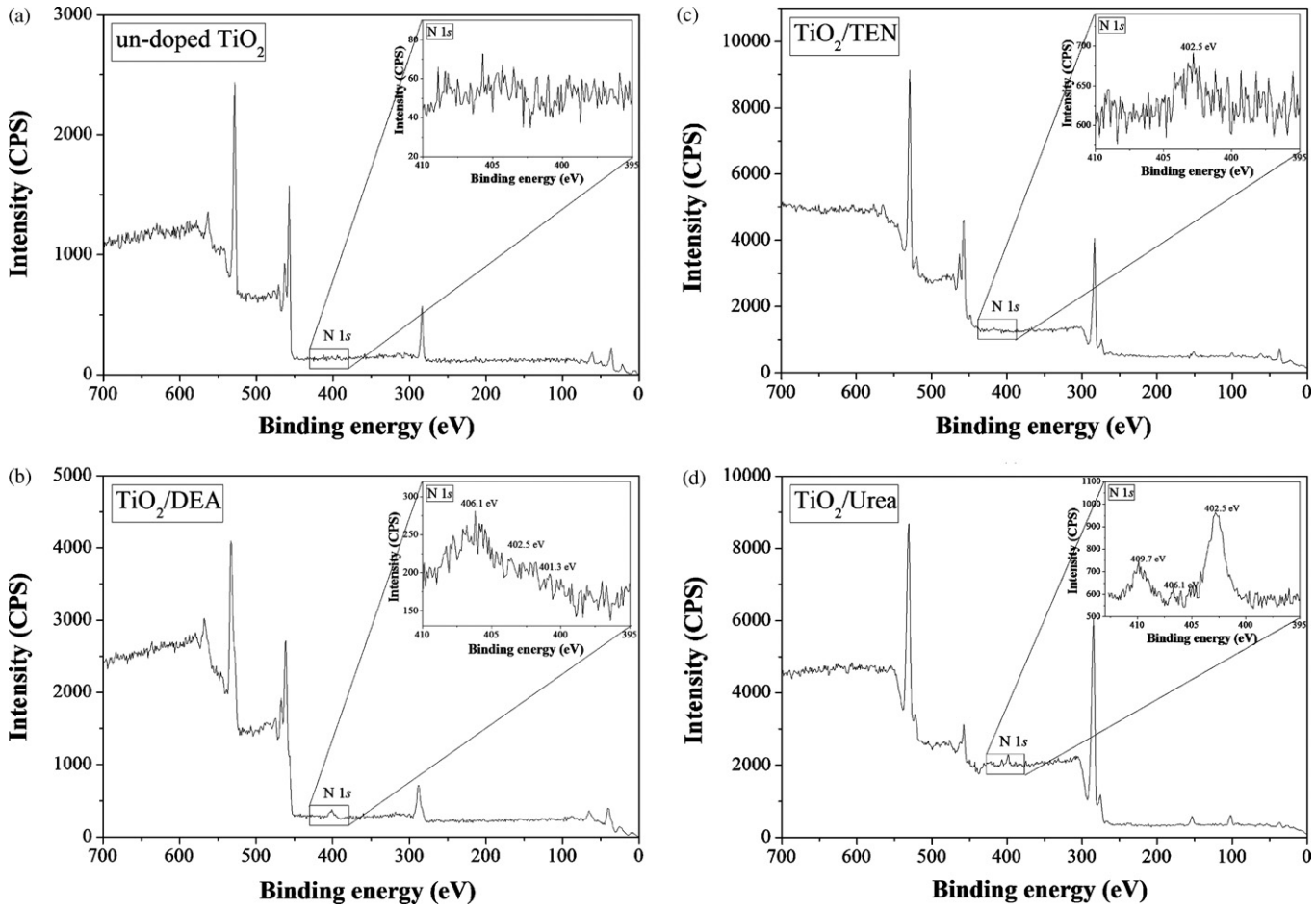

Fig. 6. XPS spectra of (a) un-doped TiO_2, (b) TiO_2/DEA, (c) TiO_2/TEN and (d) TiO_2/urea. Inset is the enlarged range of the N 1s peak.

to its smallest particle size (see Table 1). Consequently, a greater surface area provided more active sites on the TiO_2 surface for the organic pollutant to be adsorbed. In addition, the TiO_2/DEA sample was dominated by the anatase phase, which is known to be more reactive in photocatalytic processes [28,29]. Moreover, the intense absorption in the visible light range (Fig. 5) and a red-shift in the bandgap transition of the doped TiO_2 samples (Table 2) resulted in more photogenerated electrons and holes participating in the photocatalytic reactions under visible light. Therefore, more OH radicals were produced in the photocatalytic oxidation reaction and more 2-CP was degraded. The least amount of degradation was observed for un-doped TiO_2, which could have been due to highest bandgap (3.17 eV) of TiO_2, causing less OH radical production compared to the N-doped TiO_2. This lowest photocatalytic activity corresponded to the lowest visible light absorption ability of un-doped TiO_2, as shown in Fig. 5. For efficiency comparisons between TiO_2/TEN and TiO_2/urea, the efficiency of 2-CP degradation of TiO_2/TEN was higher than that of TiO_2/urea. The main reason for this effect was the higher composition of anatase to rutile of TiO_2/TEN, which yielded a higher relative number of radical formations from the surface hydroxyl species [30]. With a small portion of anatase phase and limited active surface area for photocatalytic reactions, TiO_2/urea was unable to match the 2-CP degradation observed with TiO_2/TEN. The overall percentage of degradation for 2-CP after 50 min of irradiation was 66%, 49%, 26%, 14% and 3% for TiO_2/DEA, TiO_2/TEN, TiO_2/Urea, un-doped TiO_2 and P-25, respectively.

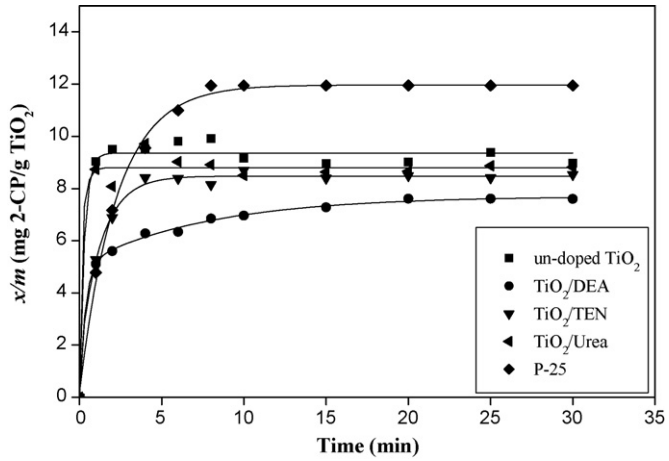

Fig. 7. Adsorption of 2-chlorophenol on the surface of N-doped TiO_2.

From kinetic studies on photocatalytic reactions of N-doped TiO_2, the reaction can be well explained by a pseudo-first-order pattern, with the following equation demonstrating the relationship of C and t:

$$\ln\left(\frac{C}{C_0}\right) = -k_{obs}t,$$

where k_{obs} is the apparent reaction rate constant, t the reaction time, C_0 the initial concentration of 2-CP in aqueous solution and C is the residual concentration of 2-CP at time t. The value of k_{obs} was determined from the slope of the graph plotted between $-\ln(C/C_0)$ and the reaction time (Fig. 8). The R^2 value for linear regression

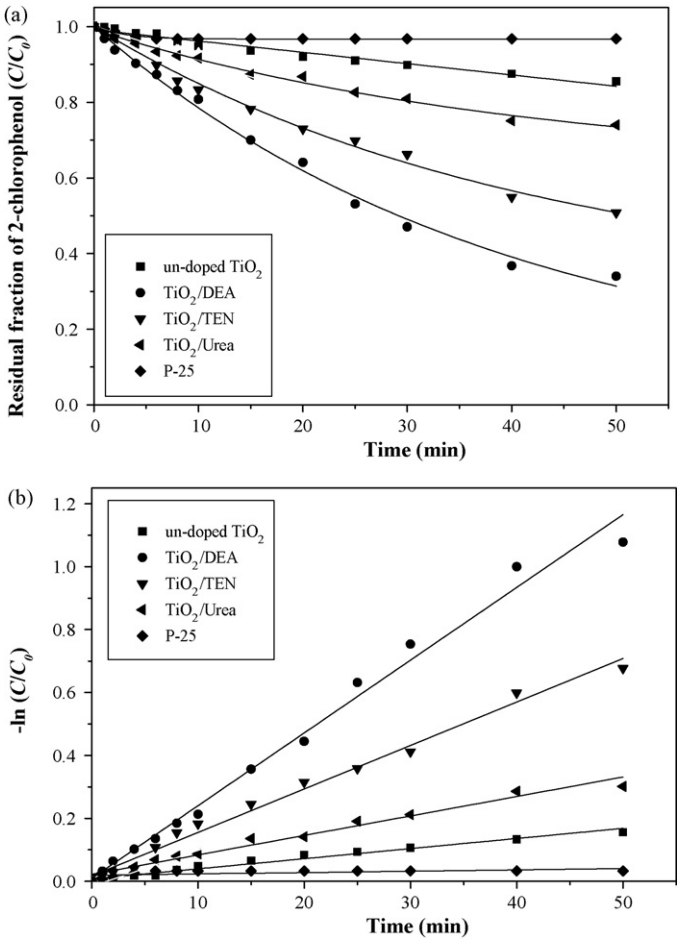

Fig. 8. Photocatalytic oxidation of 2-chlorophenol using different types of N-doped TiO_2: (a) the residual fraction plot and (b) the $-\ln(C/C_0)$ versus reaction time for 2-chlorophenol degradation using various types of N-doped TiO_2.

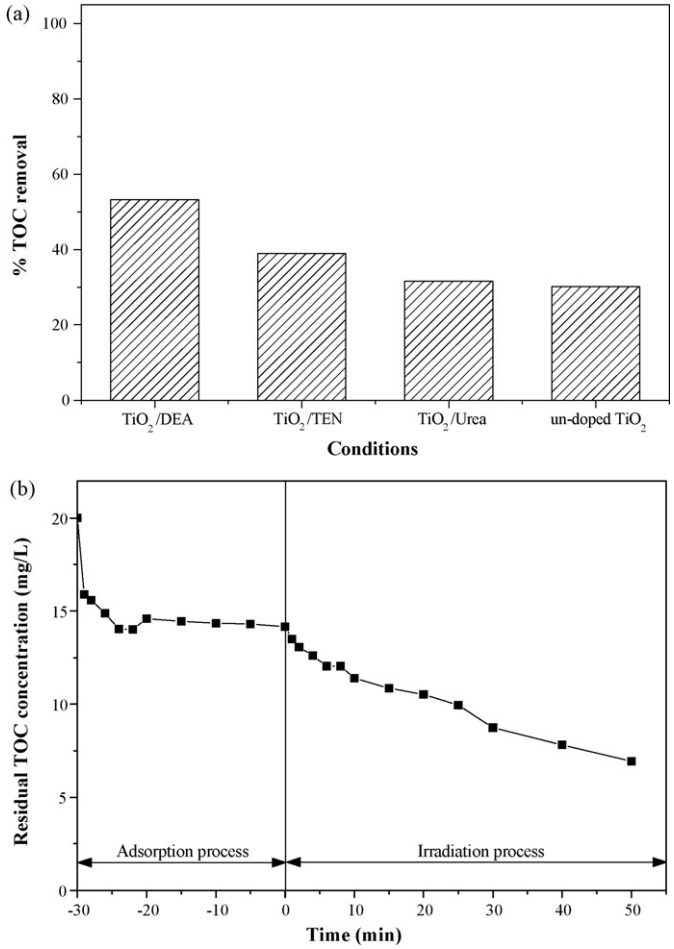

Fig. 9. (a) TOC removal percentage of 2-chlorophenol in the presence of N-doped TiO_2 and (b) reduction in residual TOC concentration with experimental time using N-doped TiO_2 with DEA.

was calculated to exhibit the tendency of the reaction, which followed the pseudo-first-order pattern. Values of initial rate, r, kinetic constant, k_{obs}, and the half-life of 2-CP, $t_{1/2}$, calculated from the pseudo-first-order equations are shown in Table 4.

Results show that within 50 min of visible light irradiation in the presence of the N-doped TiO_2 catalyst, the degradation rate of 2-CP was 0.59, 0.38, 0.22 and 0.14 mg/L-min for TiO_2/DEA, TiO_2/TEN, TiO_2/urea, un-doped TiO_2 and P-25, respectively. This pattern suggests that the reaction rate can be enhanced by nitrogen incorporation into the TiO_2 matrix. The reaction rate enhancement of the TiO_2/DEA was sixfold higher than that of the un-doped TiO_2. The rate constant of the un-doped TiO_2 reaction was only 0.35×10^{-2} min^{-1}, whereas the rate constant of the TiO_2/DEA was 2.34×10^{-2} min^{-1}. This increase may have been attributable to the intense absorption in the visible light region and a redshift in the bandgap transition of the doped TiO_2 with nitrogen dopant, as discussed previously.

3.2.3. *Mineralisation of 2-chlorophenol using N-doped TiO_2 under visible light*

The degradation percentage of 2-CP in terms of mineralisation of total organic carbon (TOC) in the presence of N-doped TiO_2 was also investigated. The initial concentration of 2-CP was 25 mg/L with an initial TOC value of 20 mg/L. The degradation percentage and mineralisation to total organic carbon of 2-chlorophenol in the presence of the four types of N-doped TiO_2 are shown in Fig. 9a. In all cases, a rapid degradation of phenol occurred and the 2-chlorophenol concentration decreased after irradiation for 30 min. Mineralisation of 2-chlorophenol in the presence of un-doped TiO_2 showed the lowest yield. Results indicate that N-doped TiO_2 with DEA provided the lowest residual concentration of TOC for 2-chlorophenol. Other types of N-doped TiO_2 can reduce TOC concentration as well. The mineralisation ability of all N-doped TiO_2 and 2-CP degradation performance can be ranked in the following order: TiO_2/DEA > TiO_2/TEN > TiO_2/urea > un-doped TiO_2. In

Table 4
Values of kinetic parameters including initial rate, r, kinetic constant, k_{obs} and half-life of 2-chlorophenol, $t_{1/2}$, based on the photocatalytic reactions of N-doped TiO_2 samples.

N-doped TiO_2	Kinetic parameters				%Removal efficiency after 50 min	Rate increase
	r (mg/L-min)	$k_{obs} \times 10^{-2}$ (min^{-1})	R^2	$t_{1/2}$ (min)		
P-25	0.12	0.11	0.9863	2094	3	–
Un-doped TiO_2	0.14	0.35	0.9818	666	14	1
TiO_2/DEA	0.59	2.34	0.9943	98	66	7
TiO_2/TEN	0.38	1.44	0.9934	160	49	4
TiO_2/urea	0.22	0.69	0.9802	333	26	2

all cases, hydroquinone was detected as the major intermediate species from 2-CP degradation occurring during irradiation process. In addition, Cl^- was also found in the residual solution after photocatalytic experiments.

Values of residual TOC concentration as a function of experimental time using the best photocatalyst, TiO_2/DEA, are shown in Fig. 9b. The residual concentration of TOC decreased gradually during the beginning of the adsorption process and remained constant during the 30 min adsorption period at approximately 14.5 mg/L TOC. During irradiation with visible light, the TOC concentration continuously declined to approximately 7 mg/L after 50 min irradiation. Note that the mineralisation process of 2-CP involved several steps before total removal of all organic intermediates was achieved. Nevertheless, photo-mineralisation greater than 94% was reached after 3 h of irradiation (with 98% 2-CP removal).

4. Conclusion

Different nitrogen dopants display differences in visible light absorption abilities, bandgap energies of the N-doped TiO_2 and consequently, photocatalytic efficiencies of TiO_2 during 2-CP degradation. XPS results show that the characteristic binding energy of the N 1s peak is above 400 eV, suggesting that nitrogen is incorporated interstitially in the TiO_2 structure. Amongst three nitrogen dopants, DEA provided the interstitial N-doped TiO_2 with highest visible light absorption ability and highest efficiency in 2-CP degradation. Results of the kinetic study show that the photocatalytic process followed a pseudo-first-order pattern. The initial rate in 2-CP degradation of the N-doped TiO_2 with DEA was 0.59 mg/L-min and the kinetic constant was 2.34×10^{-2} min^{-1} with a half-life of 98 min. The photocatalytic activity and 2-CP mineralisation ability of all N-doped TiO_2 can be arranged in the following order: TiO_2/DEA > TiO_2/TEN > TiO_2/urea > un-doped TiO_2. In all cases, hydroquinone was detected as the major intermediate species from 2-CP degradation.

Acknowledgements

Financial support from the National Nanotechnology Center, Thailand, International Foundation for Science (IFS), Sweden, and the Thailand Research Fund through the Royal Golden Jubilee Ph.D. Program (Grant No. PHD/0004/2549) to Jirapat Ananpattarachai and Puangrat Kajitvichyanukul are gratefully acknowledged.

References

[1] A. Fujishima, K. Hashimoto, T. Watanabe, TiO_2 Photocatalysis: Fundamentals and Applications, BKC Inc., Tokyo, Japan, 1999.
[2] R. Asahi, T. Morikawa, T. Ohwaki, A. Aoki, Y. Yaga, Visible-light photocatalysis in nitrogen-doped titanium oxides, Science 293 (2001) 269–271.
[3] T. Morikawa, R. Asahi, T. Ohwaki, K. Aoki, K. Suzuki, Y. Taga, Visible-light photocatalyst-nitrogen-doped titanium dioxide, R&D Rev. Toyota CRDL 40 (2005) 45–50.
[4] S. Shanmugasundaram, K. Horst, Daylight photocatalysis by carbon-modified titanium dioxide, Angew. Chem. Int. Ed. 42 (2003) 4908–4911.
[5] F. Peng, L. Cai, H. Yu, H. Wang, J. Yang, Synthesis and characterization of substitutional and interstitial nitrogen-doped titanium dioxides with visible light photocatalytic activity, J. Solid State Chem. 181 (2008) 130–136.
[6] C. Belver, R. Bellod, A. Fuerte, M. Fernández-García, Nitrogen-containing TiO_2 photocatalysts: Part 1. Synthesis and solid characterization, Appl. Catal. B 65 (2006) 301–308.
[7] D. Li, H. Haneda, S. Hishita, N. Ohashi, Visible-light-driven nitrogen-doped TiO_2 photocatalysts: effect of nitrogen precursors on their photocatalysis for decomposition of gas-phase organic pollutants, Mater. Sci. Eng. B 117 (2005) 67–75.
[8] C. Belver, R. Bellod, S.J. Stewart, F.G. Requejo, M. Fernández-García, Nitrogen-containing TiO_2 photocatalysts: Part 2. Photocatalytic behavior under sunlight excitation, Appl. Catal. B 65 (2006) 309–314.
[9] Y.Q. Wang, X.J. Yu, D.Z. Sun, Synthesis, characterization, and photocatalytic activity of $TiO_{2-x}N_x$ nanocatalyst, J. Hazard. Mater. 144 (2007) 328–333.
[10] Y. Chen, S. Zhang, Y. Yu, H. Wu, S. Wang, B. Zhu, W. Huang, S. Wu, Synthesis, characterization, and photocatalytic activity of N-doped TiO_2 nanotubes, J. Dispersion Sci. Technol. 29 (2008) 245–249.
[11] P.V. Kamat, in: D.F. Ollis, H. Al-Ekabi (Eds.), Photocatalytic Purification and Treatment of Water and Air, Elsevier Science Publishers BV, Amsterdam, The Netherlands, 1993, p. 455.
[12] P. Cheng, W. Li, T. Zhou, Y. Jin, M. Gu, Physical and photocatalytic properties of zinc ferrite doped titania under visible light irradiation, J. Photochem. Photobiol. A 168 (2004) 97–101.
[13] Standard Methods for the Examination of Water and Eastewater, 20th ed., Method 5530 A–D: Phenols, American Public Health Association, American Water Works Association, and Water Environment Federation, Washington, DC, 1998, pp. 5-40–5-44.
[14] A.M. Peiró, J.A. Ayllón, J. Peral, X. Doménech, TIO_2-photocatalyzed degradation of phenol and ortho-substituted phenolic compounds, Appl. Catal. B 30 (2001) 359–373.
[15] A.A. Gribb, J.F. Banfield, Particle size effects on transformation kinetics and phase stability in nanocrystalline TiO_2, Am. Mineral. 82 (1997) 717–728.
[16] H. Sun, Y. Bai, W. Jin, N. Xu, Visible-light-driven TiO_2 catalysts doped with low-concentration nitrogen species, Sol. Energy Mater. Sol. Cells 92 (2008) 76–83.
[17] Z. Wang, W. Cai, X. Hong, X. Zhao, F. Xu, C. Cai, Photocatalytic degradation of phenol in aqueous nitrogen-doped TiO_2 suspensions with various light sources, Appl. Catal. B 57 (2005) 223–231.
[18] N.C. Saha, H.G. Tompkins, Titanium nitride oxidation chemistry: an X-ray photoelectron spectroscopy study, J. Appl. Phys. 72 (1992) 3072–3079.
[19] D. Di Valentin, E. Finazzi, G. Pacchioni, A. Selloni, S. Livraghi, M.C. Paganini, E. Giamiello, N-doped TiO_2: theory and experiment, Chem. Phys. 339 (2007) 44–56.
[20] S. Sakthivel, H. Kisch, Photocatalytic and photoelectrochemical properties of nitrogen-doped titanium dioxide, Chem. Phys. 4 (2003) 487–490.
[21] M. Mrowetz, W. Balcerski, J. Colussi, M.R. Hoffmann, Oxidative power of nitrogen-doped TiO_2 photocatalysts under visible illumination, J. Phys. Chem. B 108 (2004) 17269–17273.
[22] K. Demeestere, A. Visscher, J. Dewulf, M.V. Leeuwen, H.V. Langenhove, A new kinetic model for titanium dioxide mediated heterogeneous photocatalytic degradation of trichloroethylene in gas-phase, Appl. Catal. B 54 (2004) 261–274.
[23] M.A. Fox, M.T. Dulay, Heterogeneous photocatalysis, Chem. Rev. 93 (1993) 341–357.
[24] R.M. Alberici, W.F. Jardim, Photocatalytic destruction of VOCs in the gas-phase using titanium dioxide, Appl. Catal. B 14 (1997) 55–68.
[25] G. Wittmann, K. Demeestere, A. Dombi, J. Dewulf, H.V. Langenhove, Preparation, structural characterization and photocatalytic activity of mesoporous Ti-silicates, Appl. Catal. B 61 (2005) 47–57.
[26] V. Ragaini, E. Selli, C.L. Bianchi, C. Pirola, Sono-photocatalytic degradation of 2-chlorophenol in water: kinetic and energetic comparison with other techniques, Ultrason. Sonochem. 8 (2001) 251–258.
[27] M. Bertelli, E. Selli, Reaction paths and efficiency of photocatalysis on TiO_2 and of H_2O_2 photolysis in the degradation of 2-chlorophenol, J. Hazard. Mater. 138 (2006) 46–52.
[28] P. Kajitvichyanukul, P. Amornchat, Effects of diethylene glycol on TiO_2 thin film properties prepared by sol–gel process, Sci. Technol. Adv. Mater. 6 (2005) 344–347.
[29] P. Kajitvichyanukul, J. Ananpattarachai, S. Pongpom, Sol–gel preparation and properties study of TiO_2 thin film for photocatalytic reduction of chromium(VI) in photocatalysis process, Sci. Technol. Adv. Mater. 6 (2005) 352–358.
[30] G. Sivalingam, M.H. Priya, G. Madras, Kinetics of the photodegradation of substituted phenols by solution combustion synthesized TiO_2, Appl. Catal. B 51 (2004) 67–76.